Environmental Science Nano

Colloidal stability of hematite nanoparticles in the presence of a common quaternary ammonium compound at environmentally-relevant concentrations

Journal:	*Environmental Science: Nano*
Manuscript ID	EN-ART-08-2023-000544.R1
Article Type:	Paper

Environmental Significance Statement

for "Colloidal stability of hematite nanoparticles in the presence of a common quaternary ammonium compound at environmentally-relevant concentrations" by Aruguete *et al*.

Quaternary ammonium compounds (QACs) are surfactants used daily in personal care products, cleaners, and as disinfectants. Due to increasing use worldwide, they are continuously released into water and soils via waste streams and sludge. Hematite (iron oxide, α-Fe_2O_3) nanoparticles (~40 nm) were exposed to a commonly-used QAC, cetyltrimethylammonium chloride (CTAC). At concentrations representative of wastewater influent (100 μg/L) and sources of concentrated QAC discharge (1000 μg/L), CTAC limited NP aggregation at air-water interfaces (AWIs). Changing the stability of iron oxide NPs may significantly impact microbial ecosystems and pollutant transport. The study results suggest that in areas with limited wastewater treatment, QACs may significantly affect the mobility and fate of iron oxide NPs, particularly in non-saturated porous zones and turbulent waters.

Colloidal stability of hematite nanoparticles in the presence of a common quaternary ammonium compound at environmentally-relevant concentrations

Deborah M. Aruguete[a], Andy Zhuang[a], Cameron Canonaco[b], Trevor Sheckler[a], Corryn Schmidt[a] and Rituraj Borgohain[c]*

[a]Department of Environmental Science, Penn State Behrend, 4205 College Drive, Erie, PA 16563, U.S.A.

[b]Department of Chemistry, Penn State Behrend, 4205 College Drive, Erie, PA 16563, U.S.A.

[c]Institute for Critical Technology and Applied Science, Virginia Tech, 325 Stanger Street, Blacksburg, VA 24061, U.S.A.

*Corresponding author contact information. E-mail: aruguete@psu.edu. Phone: +1 814 898 6895.

ABSTRACT

The fate and behavior of environmental nanomaterials can be strongly affected by organic molecules, including surfactants. Quaternary ammonium compounds (QACs) are cationic surfactants of increasing concern in the environment due to their massive everyday use and continuous release into water and soil. To examine QAC-NP interactions, ~38 nm hematite (α-Fe_2O_3) nanoparticle (NP) suspensions were mixed end-over-end with cetyltrimethylammonium chloride (CTAC), a commonly-used QAC, for 22 hours (23 °C) at environmentally-relevant concentrations of 0, 10, 100, and 1000 μg/L. Iron concentrations were measured to determine how many NPs remained in suspensions after mixing, along with characterization of the hydrodynamic diameter (Z-average) and zeta potential. Without CTAC,

the NPs were destabilized by contact with air-water interfaces (AWIs) with [Fe] decreasing from 17.65 ± 3.26 mg/L to an $[Fe]_{final}$ of 6.33 ± 2.90 mg/L. However, at 100 and 1000 μg CTAC/L, the NPs were stabilized and NP loss reduced with $[Fe]_{final}$ values of 9.50 ± 1.20 mg/L and 11.69 ± 1.25 mg/L, respectively. Measurements of surface tension and contact angles on CTAC-exposed glass were performed to explore possible stabilization mechanisms. Results suggest that in systems with air-water interfaces such as unsaturated pores or turbulent waters, elevated QAC content might alter the environmental fate and transport of iron oxide and other positively-charged NPs.

I. Introduction

Organic matter significantly affects the fate and behavior of natural and anthropogenic nanoparticles (NPs).[1] As such, understanding the effects of prevalent organic pollutants upon NPs is important for predicting NP fate and behavior in the environment. Surfactants are a major class of omnipresent organic pollutants. Levels in the environment are very likely to continue rising, as the global market for surfactants in 2020 was $39.42 billion (USD), and is projected to grow to $57.81 billion in 2028[2]. For decades, surfactants have been known to significantly alter the chemistry and physical behavior of nanomaterials[3], and can affect NP-driven processes in the environment such as transport of sorbed pollutants and chemical catalysis [4].

Quaternary ammonium compounds (QACs) are cationic surfactants of particular interest for the environment. Globally, large quantities are used daily in personal care products, disinfectants, cleaners, and laundry products as well as being used as corrosion inhibitors and emulsifiers industry and oil operations.[5] The COVID-19 pandemic increased consumer interest in hygiene and disinfection, leading to increased demand and use of QACs.[2, 6] With modern

wastewater treatment, only ~90% of QACs are removed from influent water[6], meaning that QACs are continually entering environmental systems. As QAC use increases globally, more will enter the environment.

The interaction of mineral colloids with QACs, including NPs (*e.g.* clay) has been examined heavily for applications such as mineral refinement[7] and oil recovery[8], but less is known about environmentally-relevant levels of surfactants and their interaction with mineral nanoparticles. In particular, the interaction of positively-charged nanoparticles such as iron oxide colloids[9, 10] with cationic surfactants remains to be explored in an environmental context. Thus, the goal of this study was to measure the stability of a positively-charged mineral NP suspension exposed to a common QAC at environmentally-relevant concentrations. Synthesized hematite NPs (~40 nm) were exposed to the commonly-used QAC cetyltrimethylammonium chloride (CTAC, also known as hexadecyltrimethylammonium chloride) at concentrations of 0 μg/L, 10 μg/L (0.031 μM), 100 μg/L (0.31 μM) and 1000 μg/L (3.13 μM) for 22 hours. These concentrations were selected based upon measurements of QACs in the environment and wastewater[5, 6]. The amount of NP remaining suspended in solution at varying [CTAC] was followed via elemental analysis for iron. The NP aggregation state was determined with dynamic light scattering (DLS). To gain insight into possible mechanisms by which CTAC affected stability, trials were run with an air-water interface (+AWI) and without an AWI (-AWI). Furthermore, the zeta potential, the surface tension of CTAC solutions and the contact angles of CTAC-exposed borosilicate were determined.

II. Materials and methods

1. Reagents

Ultrapure (18.2 MΩ · cm resistivity) water was used for all experiments and rinsing unless otherwise mentioned. High-purity (Fisher TraceMetal™ grade) hydrochloric acid (HCl) and nitric acid (HNO_3) were used for synthesis, analysis and cleaning. The purity of any other reagents used was at a minimum ACS grade unless otherwise specified.

2. NP synthesis and purification

Hematite NPs were synthesized via the forced hydrolysis of an iron salt following the method of Madden *et al* (2006). Five hundred milliliters of 0.002 M HCl were brought to a boil in a 1 L Erlenmeyer flask. Subsequently, 4.04 g of $Fe(NO_3)_3 \cdot 9H_2O$ (Supelco EMSURE® grade, >99%, MillporeSigma, Burlington, MA USA) were added. The mixture was magnetically stirred at 85 °C for 7 days, periodically replacing evaporated water, then allowed to cool to room temperature. A portion of the synthesized NPs were then dialyzed at room temperature with Spectra/Por® 1 dialysis membranes with a 6-8 kDa MWCO (Spectrum Chemical Mfg Co., New Brunswick, NJ USA). The conductivity of the dialysis water was measured daily and the water was replaced until the conductivity was equal to that of the ultrapure water (≤ 2.5 μS). All NP suspensions were stored at 4 °C in the dark.

3. Materials characterization

Powder X-ray diffraction (XRD) was used to characterize the iron oxide crystal phase present. Nanoparticle solutions were concentrated down to ~200-500 μL using Amicon Ultra-15 Centrifugal Filter Units with a 30 kDa MWCO (MilliporeSigma, Burlington, MA USA). Subsequently, these highly concentrated solutions were deposited onto zero-background XRD sample substrates and allowed to fully air-dry. XRD data was collected using an Empyrean

Nano Edition multipurpose diffractometer (Malvern Panalytical, Westborough, MA USA) equipped with a Cu source (λ Cu Kα = 0.15406 nm).

A JEOL 2200 Scanning/Transmission Electron Microscope (S/TEM) operating at 200 kV was used to obtain bright field TEM images. TEM bright field images were acquired with a Gatan Ultrascan 1000XP CCD camera. TEM analytical work was performed at Virginia Polytechnic Institute and State University in the Nanoscale Characterization and Fabrication Laboratory. Size determination was performed by measuring the areas of 50 NPs using ImageJ (US National Institutes of Health, Bethesda, MD, USA).

4. Stability experiments

The stability of NPs exposed to different mixing conditions was monitored in 20 mL EPA Level 100 screw-cap borosilicate glass vials (Thermo Fisher Scientific, Waltham, MA USA). Contaminants in the vials, namely trace organics (*e.g.* detergent) and residual NPs from prior experiments caused problems with reproducibility; thus a thorough cleaning procedure was developed and is detailed here. Vials were first gently scrubbed with Alconox detergent (Alconox Inc., White Plains, NY USA) and rinsed with deionized water (not ultrapure). After that, approximately 2-5 mL of concentrated HCl was added to coat the vial walls and dissolve any residual Fe_2O_3 NPs, then rinsed at least 6x with ultrapure water. To remove organics, the vials were then soaked in an oxidizing solution of 19 g/L ammonium persulfate in 98% sulfuric acid for at least 12 hours. (Warning! Concentrated acids are dangerous and should only be handled wearing appropriate protective equipment, fume hoods, and with $NaHCO_3$ to neutralize spills. The H_2SO_4-ammonium persulfate mixture is both very acidic and highly oxidizing. Do not introduce organic solvents or compounds as forceful reactions may take place.)

After soaking, the glass vials were then rinsed with water at least 6x to remove any residual solution. They were also visually inspected to ensure that the rinsing water entirely wet the glass, indicating the elimination of most trace organics. The vials were tapped to remove water and allowed to air-dry with lab tissue coverings to prevent contamination. The vial caps (lined with PTFE-faced foamed polyethylene) were rinsed 6x with water, then tapped dry. To limit contamination, caps were only used once for an experiment, and replenished with equivalent fresh caps (DWK Life Sciences, Millville, NJ USA).

Freshly dialyzed NP suspensions were diluted with water to have an absorbance of 0.5 at 500 nm measured using a ThermoSpectronic Genesys 20 absorption spectrometer (Thermo Fisher Scientific), corresponding to an $[Fe]_{initial}$ of 17.65 ± 3.26 mg/L. As NPs in any solvent can change in size distribution over time, the NPs for these experiments were used only within a month after their synthesis. Figure 1 provides a schematic of experiments. To perform +AWI trials, vials were half-filled with the diluted suspension (10 mL); to perform -AWI trials, vials were completely filled and checked to confirm there were no air bubbles present. For each trial with CTAC, immediately prior to mixing, an aliquot of 10^3, 10^4 or 10^5 µg CTAC/L stock solution was added to the iron NP suspension, resulting in [CTAC] = 10 µg/L (0.03 µM), 100 µg/L (0.3 µM) and 1000 µg/L (3 µM). These concentrations were chosen to span the range of [QAC] measured in environmental samples and wastewater-associated waters (influent, effluent)[5, 6]. The vials were then capped and placed on a Fisherbrand™ Multi-Purpose Tube Rotator (rotary mixer) for 22 hours at 30 rpm.

To quantify the stability of NP suspensions, analyses were performed to determine the amount of NPs remaining suspended after mixing (as opposed to those that were deposited on vial walls). Within an hour after mixing was complete, aliquots of the suspension were

withdrawn for analyses to determine the amount of NPs remaining in suspension. To limit the introduction of NPs deposited upon vial surfaces and the possible introduction of NPs on top of the AWI, aliquot collection was performed carefully below the surface of the liquid in the center of the vial, as shown in Figure 1. From each vial, 0.5 mL of the suspension were withdrawn and the absorbance of this aliquot determined at 500 nm. Such measurements served as a rapid means for inspecting the effect of a treatment upon NP suspension stability, as A_{500} values were found to be positively correlated with [Fe]. As optical absorbance of NP suspensions is affected by concentration, particle size/aggregation, and other size-influenced physicochemical parameters, it was only utilized as a semiquantitative measurement. The absorbance measurements are provided in the ESI, with Figure S1 being a box-and-whisker plot of A_{500} for different treatments, and Table S3 containing averages, standard deviations, medians and sample sizes.

5. Elemental analysis of suspensions for iron

To determine how much Fe remained in the suspension, namely the amount of hematite NPs remaining, samples were analyzed as follows. Within an hour after mixing was complete, two milliliters of the suspension (~0.5-1 cm below the surface) were withdrawn per the procedure described in the prior section, then prepared for analysis with a MARS6 microwave digester (CEM Corporation, Matthews, NC, USA) following the CEM Ferric Oxide method[11]. (This digestion requires concentrated acids; please see safety information in the Stability Experiments section above.). The digests were then diluted with 5%(v/v) HNO_3 (20x dilution factor of digest; 300x dilution factor for original suspension) and stored at 4°C in the dark until analysis. Subsequently, elemental analysis for iron was conducted using an Agilent 7900

inductively-coupled plasma mass spectrometer (ICP-MS, Agilent Technologies Inc., Santa Clara, CA, USA). Operating conditions and a discussion regarding preferred iron isotopes are in Part I of the Electronic Supplementary Information.

6. Determination of ionic iron in suspensions

To examine whether the NP suspensions showed signs of NP dissolution, 3 mL aliquots were collected from two samples each of the following: freshly-sonicated NP prior to mixing and -AWI NP suspensions after 22h mixing at [CTAC] = 0 and 1000 μg/L. Each aliquot was filtered with 3 kDa MWCO Amicon® Ultra-4 centrifugal units (MilliporeSigma, Burlington, MA USA). This MWCO is recommended for NP with a minimum size of 1 - 1.5 nm[12], thus acting as an effective filter for ~38 nm NPs, even those with a broad size distribution. Due to limited availability, after filtration, 0.5 mL of the filtrate was diluted to 10 mL with 5%(v/v) HNO_3 (20x dilution). Detection limits for iron were calculated utilizing Agilent MassHunter version 5.1[13].

7. Characterization of NP aggregation state and zeta potentials

The aggregation state and zeta potentials of colloidal NP subjected to different treatments were characterized via dynamic light scattering (DLS) and zeta potential measurements using a Zetasizer Nano ZS equipped with a universal dip cell (Malvern Instruments, Southborough, MA USA). Measurements were taken at 25 °C on freshly-sonicated NPs before treatment (pre-mixing), then on NPs as soon as possible after mixing was complete (1 mL aliquot per sample).

8. Surface tension and contact angle measurements

To elucidate possible mechanisms behind the effect of CTAC upon NP stability, the surface tension of ultrapure water and solutions with [CTAC] = 10, 100, and 1000 μg/L was determined. As [CTAC] increased, the surface tension decreased. However, as the change was minimal, CTAC concentrations of 10^4, 10^5, and 10^6 μg/L were also analyzed to determine if there was any trend. Surface tension was measured using the pendant drop technique using an optical tensiometer (Theta Flow, Biolin Scientific, Finland) with OneAttension software. The images of the drop were recorded with a black-and-white high-resolution (2592 × 2048) digital camera over 10 seconds (101 measurements) and the surface tension obtained by iterative fitting of the shape of the drop with the Laplace equation. The temperature was maintained at 23.7 ± 0.2°C.

To determine whether CTAC significantly modified the reaction vial wall affinity for NPs, borosilicate microscope coverslips (Thermo Fisher Scientific) were immersed in water and solutions with [CTAC] = 10, 100, 1000, 10^4, 10^5, and 10^6 μg/L overnight, rinsed three times with ultrapure water, and allowed to dry. The three highest [CTAC] were measured for the same reasons as in the surface tension measurements. Droplets (10 μL) of ultrapure water were placed on the borosilicate surfaces to determine contact angles using the sessile drop technique. A Ramé-Hart model 250 goniometer was used for the measurements using a level surface (0 ° tilt angle). A minimum of five droplets (10 contact angles) were measured for each substrate aside from 100 μg CTAC/L – exposed substrates (three droplets measured). Each droplet placed onto a separate part of each substrate. The temperature was maintained at 23.7 ± 0.2°C. Measurements of the contact angles on images were performed using the DROPImage Advanced program version 3.22.03.0 (Ramé-Hart Instrument Co., Succasunna, NJ USA).

9. Statistical analysis

To assess the statistical significance (95% Confidence Intervals) of measurements between different treatments, all datasets for [Fe], Z-average size, polydispersity index (PdI), and zeta potential were subjected to the Andersen-Darling Test for normality ($\alpha = 0.05$). As multiple datasets were non-normally distributed, Kruskal-Wallace testing was performed, followed by Mann-Whitney tests for pairwise comparisons. To maintain an overall family error rate of $\alpha = 0.05$, the significance threshold for individual pairwise comparisons was subjected to the Bonferroni Correction. This correction entails dividing the overall family error rate $\alpha = 0.05$ by the number of pairwise comparisons. For the elemental analysis data, there are 36 pairings, so the significance threshold is $p \leq 0.001$. For the DLS and zeta potential data, the -AWI 10, 100 and 1000 samples were not included in the family analysis due to small sample sizes, meaning there were only 15 pairwise comparisons, resulting in a significance threshold of $p \leq 0.003$. Thus, individual pairwise comparison was tested at the corresponding level of significance to determine which treatments were different. The statistical analysis procedures above were also used for surface tension and contact angle measurements. All analyses were performed using the Minitab Web App (v. 21.3.1).

III. Results and Discussion

1. Characterization of NPs

Figure 2 (top) presents a representative TEM image of the NPs with a rhombohedral morphology similar to those observed in earlier work[14] utilizing this synthesis. The average size of the NPs (circular equivalent diameter) was 37.79 ± 5.00 nm. On the bottom of Figure 2, XRD data show that the NPs consist of hematite, and is consistent with XRD of hematite NPs

synthesized in a similar fashion.[15] The indexed reflections are provided, calculated based upon unit cell parameters.[16, 17]

2. Potential for NP dissolution

Nanoparticle dissolution processes were considered, as significant dissolution could be the reason behind elevated [Fe] rather than changes in colloidal stability. As such, ultrafiltration was performed to separate NPs from any ionic Fe (this could in theory include iron oxide clusters < 1 nm in size). The iron concentrations of the ultrafiltrates from pre-mixing NPs, as well as NPs mixed for 22 h (-AWI at [CTAC] = 0, 1000 μg / L) were all found to be below the detection limit of 0.7835 μg Fe / L. Multiplying the detection limit concentration by the dilution factor of the filtrate (20×) results in an upper limit of $[Fe]_{ionic}$ = 15.67 μg Fe / L, which is ≤ 0.1% of the average [Fe] for the pre-mixing and post-mixing -AWI samples. These results suggest that NP dissolution was not likely to be a process significantly affecting NP stability.

Even without the above results, consideration of other driving forces behind dissolution is important. In other systems, surfactants could form metal complexes, thus potentially driving NP dissolution. In this study, while CTA^+ cations would not act as Lewis bases to form Fe coordination complexes, the accompanying Cl^- ions potentially could. However, prior work suggests that under the conditions of this experiment, with a maximum $[Cl^-]$ of 1.56×10^{-6} M, hydrated Fe^{3+} would be the predominant species[18], suggesting that the significant formation of chloro-complexes is unlikely.

2. Effect of air-water interface (AWI) upon colloidal stability

Characterization data for NP suspensions prior to mixing and after all treatments (-AWI and +AWI at [CTAC] = 0, 10, 100 and 1000 μg /L) are presented as follows. Figure 3 displays the intensity-based particle size distributions (PSDs) from DLS. Figure 4 presents (A) box-and-whisker plots of [Fe], (B) Z-average sizes from DLS and (C) zeta potentials. The mean values, standard deviations and sample sizes are provided in Table 1. The individual *p*-values for pairwise dataset comparisons are provided in the Part II of the Electronic Supplementary Information, Tables S4 – S9.

The aggregation state of the -AWI NP suspensions did not change significantly ($p > 0.003$ for Z-averages) from the NP suspensions prior to mixing, as is evident in the -AWI PSDs (Fig. 3(e)-(h)) relative to the starting PSD (Fig. 3 bottom). The mean Z-average size prior to mixing was 139.14 ± 3.26 nm; after mixing without an AWI, the mean Z-average was 153.43 ± 7.18 nm. The PSD does not appear to broaden; PdI is 0.116 ± 0.016 for the pre-mixing NPs and 0.145 ± 0.021 for the -AWI nanoparticles. Correspondingly, elemental analysis results (Fig. 4A) also did not show significant change, as the average -AWI [Fe] (17.30 ± 3.26 mg/L) was not significantly different ($p = 0.738$) from the starting [Fe] (17.65 ± 3.26 mg/L). The zeta potentials were positive as would be expected for hematite (particularly synthetic[9]), given that the point of zero charge (PZC) / isoelectric point (IEP) is between pH ~7-9[10, 19, 20] and the pH of the suspensions was ~5.6. The zeta potentials from both treatments were not significantly different ($p = 0.927$), with values of 37.7 ± 6.0 mV for the pre-mixing NPs and 34.3 ± 2.2 mV for -AWI NPs.

Exposure to an AWI destabilized the NP suspensions. After 22 h of mixing, the +AWI vials had a reddish tint visible on the vial walls and the caps, indicating that NPs were deposited onto these surfaces. The [Fe] remaining in suspension from the +AWI samples decreased

significantly from the starting concentration ($p < 0.0005$), with a mean [Fe] of 6.33 ± 2.90 mg/L. The +AWI PSD for the NPs remaining in the suspension (Fig. 3(a)) shifted upwards, with one major peak at 342 nm, and another minor peak at 4800 nm. The Z-average size increased to 655.13 ± 229.16 nm (this Z-average size should be interpreted with caution as there were signs of number fluctuation, possibly due to the settling of very large aggregates; this is discussed in section IV of the ESI). As expected, since no other additives were present to sorb onto NP surfaces, the zeta potential for the +AWI treatment was still positive (32.4 ± 5.2 mV) and was not significantly different from the pre-mixing NPs ($p = 0.210$) or the -AWI NPs ($p = 0.121$).

These results are consistent with previously observed destabilization of colloids in the presence of air-water interfaces[21], used extensively for applications such as froth flotation in the refinement of ore. Williams and Berg elegantly summarized this process leading to particle aggregation[21] as follows: (1) particles move towards AWI via Brownian motion (in this study, there are additional driving forces due to mixing) , (2) particles adsorb to AWI, (3) particles rupture the water surface, becoming de-wetted, and (4) particles are trapped on surface. The contact angle of the particle material will control the degree of de-wetting. Finally, as the density of particles on the water surface increases, aggregation occurs.

3. Effect of CTAC upon colloidal stability

3.1 Effect of CTAC concentration

Vials carrying +AWI 10 NP suspensions still had visible deposits of NPs upon the caps and vial walls, although to a lesser extent than the +AWI (no CTAC) vials. For [CTAC] = 100 and 1000 μg/L, visible deposits were primarily on the caps. The [Fe] in the suspensions were consistent with these observations. The +AWI-10 suspensions had [Fe] = 7.83 ± 2.75 mg/L,

which was not significantly different from the +AWI suspensions ($p = 0.057$), although the +AWI 10 PSD (Fig. 3(b)) shifted to lower sizes than for +AWI NP only suspensions (Fig. 3(a)), with a maximum intensity at 295 nm. This suggests that while both the +AWI and +AWI 10 treatments did result in NP aggregation, aggregates were smaller when CTAC was present at 10 μg/L. With an increase of [CTAC] to 100 μg/L, a degree of colloidal stabilization occurred, with a suspension [Fe] of 9.50 ± 1.20 mg/L, a significant ($p < 0.0005$) increase relative to the +AWI treatments. When [CTAC] = 1000 μg/L , the average [Fe] for the +AWI treatments was 11.69 ± 1.25 mg/L. The Z-average sizes were similar to those from the pre-mixing and -AWI treatments ($p \geq 0.075$). The difference between [Fe] for the +AWI-100 versus the +AWI-10 treatments trended towards significance at $p = 0.004$, but it did not meet the Bonferroni-corrected significance threshold of $p \leq 0.001$.

3.2. CTAC-induced colloidal stabilization: investigation of possible mechanisms

3.2.1. Interaction between model mineral surfaces (vial walls) and CTA^+

One possible cause for CTA^+ leading to less aggregation and/or deposition of NPs could be surface modification of the vial interior. The borosilicate inner walls of the reaction vials are analogous to minerals and anthropogenic materials that could interact with QACs in the environment. The PZC of borosilicate has been measured to be 3.00 ± 0.26[22], similar to SiO_2 minerals. As the NP suspensions in this study have a pH of ~5.6, it is assumed that the vial walls were negatively-charged and electrostatically attractive to the positive polar head group of CTA^+. Cetyltrimethylammonium cation (CTA^+) can sorb to SiO_2 at pH 5[23] and pH 6.5[24]. Sorption of CTA^+ to vial walls could make them hydrophobic, decreasing the affinity of the borosilicate surface for positively-charged NPs.

A simplified calculation approximating the maximum possible coverage of the inner vials walls suggests that at [CTAC] values of 100 and 1000 μg/L, significant coverage would theoretically be possible. In this calculation, it is assumed that the polar headgroup of CTA^+ has an area of 0.68 nm^2 [25] and that the vial is a cylinder with an inner diameter of 2.5 cm and a height of five centimeters. For 10 mL of solution in a vial, assuming all CTAC sorbed to the glass walls, at 10 μg CTAC/L, 2.61% of the glass vial surface would be covered; at 100 μg CTAC/L, 26.1% would be covered; and at 1000 μg CTAC/L, the coverage would be complete (261% of glass surface).

Whereas prior work and the calculation above indicate the possibility of CTA^+ sorption, the effects of any such sorption could not be quantified with contact angle measurements. Contact angles on borosilicate class exposed to [CTAC] = 0 – 1000 μg/L are shown in Figure 5 (black circles) and mean contact angle values provided in Table 2. There were no significant differences between the measured contact angles on borosilicate exposed to solutions with [CTAC] = 0, 10, 100 and 1000 μg/L. This was inconsistent with visual observations; when rinsing the substrates with water, the water did not cling to CTAC-exposed borosilicate as well as it did to the borosilicate controls (not exposed to CTAC).

The contact angle results do not necessarily indicate that no CTAC sorbed to the vial walls, as the dried, CTAC-exposed borosilicate substrates are not an exact facsimile of the conditions of the vial walls. It is clear from the contact angle changes at higher [CTAC] that CTA^+ can interact with borosilicate surfaces. However, for [CTAC] = 0 – 1000 μg/L, no measurable correlation between hydrophobicity and NP stabilization was observed. More sensitive surface characterization methods may be required to offer further insight.

3.2.2. Reduction of surface tension at the AWI

Another possible mechanism behind colloidal stabilization is the reduction of surface tension at the AWI, which would decrease the energetic barriers for NPs to return to the bulk solution. The work required to detach a hydrophobic particle from the AWI and return to the bulk solution[21, 26] can be expressed as

$$W_{detachment} = \sigma_{LA}(A_{SA}(\cos\theta) - A_{disp}) \qquad \text{(equation 1)}$$

in which σ_{LA} is the surface interfacial free energy of the AWI, A_{SA} is the area of the solid-air interface (area of particle above water), θ is the contact angle of the particle material, and A_{disp} refers to the area of water displaced by the particle.

The σ_{LA} values used for this study were obtained by measuring surface tension at 0, 10, 100, 1000, 10^4, 10^5 and 10^6 μg/ L and are shown in Figure 5 (black squares for environmentally-relevant concentrations) with mean values provided in Table 2. Surface tension is decreased at 1000 μg CTAC / L relative to the lower CTAC concentrations ($p < 0.0005$). However, surface tension at 100 μg CTAC/L was not distinguishable ($p = 0.052$) from the CTAC-free controls or the 10 μg CTAC/L trials ($p = 0.251$), even though colloidal stability was increased at 100 μg CTAC/L. The difference in surface tension between the 0 and 1000 μg CTAC/L solutions was 0.31 ± 0.26 mN/m.

The magnitude of this difference and the fact that the σ_{LA} term is multiplicative rather than exponential (equation 1) suggest that surface tension might not be the dominating cause of the CTAC in the range from 0 – 1000 μg/ L. A caveat to this argument is the possibility of a synergistic interaction between NPs and CTAC that would lower σ_{LA} further. This occurred for

negatively-charged silica NPs exposed to anionic surfactants.[27, 28] However, those results may not be applicable as the surfactant concentrations and weight % of NPs in this study are >200 – 1000x lower than in the aforementioned work. As with the contact angle measurements, a more sensitive method for determination of surface tension may provide more conclusive insights.

3.2.2. Charge alteration of AWI by CTAC

In pure water at most pH values, the zeta potential of the AWI is negative[29]. Ionic surfactants generally will change the AWI charge according to the charge of the polar head, with cationic surfactants making the AWI positive.[30] For CTA-bromide (CTAB) solutions with concentrations close to those used for those study, it was inferred that at 0.05 μM and 0.5 μM, CTA^+ sorption at the AWI lowered the magnitude of the negative potential at the diffuse electric layer, even nullifying it.[31] With increasing [CTAB], it was concluded that the potential would become positive.

A positively-charged AWI would likely repel positively-charged hematite NPs. If this happened, fewer NPs would adsorb to the AWI. Therefore, fewer NPs would be trapped at the AWI, resulting in less NP aggregation. This mechanism is consistent with a recent study that found electrostatic repulsion between NPs and an AWI with the same charge. Tian and co-workers[32] studied polymeric NPs (~75 nm), determining their rate of diffusion to the AWI by monitoring surface tension of the NP suspensions over time. Using CTAB, both the AWI and the NPs became positively-charged, and the rate of NP diffusion to the AWI was significantly slowed. The reduced rate also occurred when CTAB was used to make both NPs and the AWI negatively charged, but did not occur when a neutral surfactant was used.

3.2.4. CTA^+ coating or encapsulation of NPs

Natural dissolved organic matter can coat NPs and decrease aggregation[1], as well as anthropogenic surfactants[3]. NP coating often involves non-covalent bonding of the polar head of a surfactant to the NP surface. The binding of CTA^+ to colloid surfaces has long been observed for minerals commonly carrying negatively-charged surfaces such as clays[33] as well as other nanomaterials such as gold NPs[34]. However, for this system, given the positive charge of hematite NPs under the conditions used, it is unlikely that the positively-charged headgroups on CTA^+ molecules would have a strong affinity. Encapsulation of the hematite NPs into surfactant micelles might also occur, although the critical micelle concentration (CMC) of CTAC was measured to be 1580 μM[35] (prior literature ~1300 μM[35]). Thus, the CMC is 461x greater than the maximum [CTAC] used in this study (1000 μg/L, 3.13 μM).

If CTAC coated or encapsulated the NPs, this would likely result in a greater hydrodynamic diameter and consequently a shift in the DLS PSD (thus an increase in Z-average). This has been previously observed for NPs with coatings[36]. However, the Z-average sizes for +AWI-100 and +AWI-1000 suspensions (156.27 ± 8.92 nm and 150.77 ± 7.18 nm) were not significantly different from the aforementioned Z-average sizes prior to mixing or from the -AWI treatments. The CTAC-spiked -AWI suspensions behaved similarly, with mean Z-average sizes ranged from 130.18 ± 0.61 nm to 141.38 ± 22.40 nm, again displaying relatively small differences with the suspension before mixing. Given these results, it is unlikely that surfactants are associating closely with NPs, and thus unlikely that the NP colloids are stabilized due to encapsulation or coatings.

IV. Conclusions and Implications for Environmental Systems

Specific conclusions and suggestions for future work based upon these studies are as follows. Results for CTAC indicate that it is possible for QAC cationic surfactants to affect the behavior of positively-charged hematite NPs. Specifically, the presence of CTAC limited AWI-induced destabilization of hematite NP suspensions. This occurred at concentrations corresponding primarily to what is found in polluted waters (WWTP influent, hospital effluent, unprocessed sewage, pore spaces in soil amended with sludge). Thus, for systems where positively-charged mineral colloids are likely to play a role, *e.g.* systems with other iron oxides and various aluminum oxide[20] NPs, the potential for QAC pollution to affect NP fate and transport may be significant. The results of the +AWI and -AWI treatments suggest that the physicochemical effects of QACs upon positively-charged NPs may be most prominent in systems with AWIs, such as turbulent waters or unsaturated porous media.

The mechanisms behind the stabilizing effect of CTAC remain unclear, although some can be ruled out. Based upon prior work as well as DLS data, stabilization via coating or encapsulation of NPs is unlikely. Also, changes in NP size distribution due to dissolution and Ostwald ripening are not likely based upon [Fe] measurements of ultrafiltrate (NPs removed by ultrafiltration). However, the role of CTAC-induced surface tension changes is unknown, as tensiometry measurements only detected a significant change in surface tension (relative to pure water) at a [CTAC] of 1000 μg/L. As such, any correlation (if present) between surface tension at lower [CTAC] and NP suspension stability could neither be confirmed nor excluded. Similarly, any correlation between the hydrophobicity of the vial walls and NP suspension stability could not be determined, because no significant change in contact angle (relative to the plain borosilicate substrates) could be measured for substrates exposed to [CTAC] = 10, 100, and 1000 μg/L. It is possible that more sensitive measurement techniques for surface tension and

hydrophobicity may be warranted for future work. Alternatively, experiments to examine other possible mechanisms such as CTAC-induced changes in the charge of the AWI could be considered.

Finally, in considering the environmental implications of this work, it is important to note that there is enormous variety among the QACs utilized within household products and industry. Thus, even though CTAC was found to only induce NP stabilization at these concentrations, it is possible that commonly used QACs such as benzalkonium or cetylpyridinium chloride could have effects at lower concentrations. Further work is necessary to explore such possibilities.

V. Conflicts of Interest

There are no conflicts of interest to declare.

VI. Acknowledgments

D.M.A. acknowledges Penn State Behrend startup funding. She thanks the Orris C. Hirtzel and Beatrice Dewey Hirtzel Memorial Foundation and Lake Erie Research Institutes for supporting instrumentation. She thanks Dr. Michael Justik (Penn State Behrend) and Dr. Michael Hochella (Pacific Northwest National Laboratory) for helpful discussions, and Dr. Sheri Singerling, Dr. Weinan Leng, Dr. Kaiwu Huang, Dr. Jing Zhao and Mr. Patrick Finley (Virginia Tech) for assistance with measurements. A.Z. and C.C. acknowledge support from Penn State Behrend Summer Undergraduate Research Grants.

Surface tension measurements were made possible by the use of Virginia Tech's Materials Characterization Facility, a joint venture of the Institute for Critical Technology and Applied Science, the Macromolecules Innovation Institute. Contact angle measurements were

made at the Center for Advanced Separation Technologies (CAST) at Virginia Tech. The acquisition of transmission electron microscopy, dynamic light scattering and zeta potential data was supported by the Nanoscale Characterization and Fabrication Laboratory and the Virginia Tech National Center for Earth and Environmental Nanotechnology Infrastructure (NanoEarth), a member of the National Nanotechnology Coordinated Infrastructure (NNCI), supported by NSF (ECCS 1542100 and ECCS 2025151).

VII. References

1. A. Philippe and G. E. Schaumann, Interactions of Dissolved Organic Matter with Natural and Engineered Inorganic Colloids: A Review, *Environmental Science and Technology*, 2014, **48**, 8946-8962.

2. F. B. Insights, *Surfactants Market Size, Share, and COVID-19 Impact Analysis By Type (Anionic, Nonionic, Cationic, and Amphoteric), By Application (Home Care, Personal Care, Textile, Food & Beverages, Industrial & Institutional Cleaning, Plastics, and Others), and Regional Forecast, 2021-2028*, Report FBI102385, Fortune Business Insights, 2021.

3. H. Heinz, C. Pramanik, O. Heinz, Y. Ding, R. K. Mishra, D. Marchon, R. J. Flatt, I. Estrela-Lopis, J. Llop, S. Moya and R. F. Ziolo, Nanoparticle decoration with surfactants: Molecular interactions, assembly, and applications, *Surface Science Reports*, 2017, **72**, 1-58.

4. M. F. Hochella Jr., D. M. Aruguete, B. Kim and A. S. Madden, in *Nature's Nanostructures*, eds. A. S. Barnard and H. Guo, Pan Stanford Publishing Pte. Ltd., 2012, ch. 1, pp. 1-42.

5. W. A. Arnold, A. Blum, J. Branyan, T. A. Bruton, C. C. Carignan, G. Cortopassi, S. Datta, J. DeWitt, A.-C. Doherty, R. U. Halden, H. Harari, E. M. Hartmann, T. C. Hrubec, S. Iyer, C. F. Kwiatkowski, J. LaPier, D. Li, L. Li, J. G. Muñiz Ortiz, A. Salamova, T. Schettler, R. P. Seguin, A. Soehl, R. Sutton, L. Xu and G. Zheng, Quaternary Ammonium Compounds: A Chemical Class of Emerging Concern, *Environmental Science and Technology*, 2023, **57**, 7645-7665.

6. P. I. Hora, S. G. Pati, P. J. McNamara and W. A. Arnold, Increased Use of Quaternary Ammonium Compounds during the SARS-CoV-2 Pandemic and Beyond: Consideration of Environmental Implications, *Environmental Science and Technology Letters*, 2020, **7**, 622-631.

7. Y. Xing, M. Xu, X. Gui, Y. Cao, M. Rudolph, H.-J. Butt and M. Kappl, The role of surface forces in mineral flotation, *Current Opinion in Colloid and Interface Science*, 2019, **44**, 143-152.

8. Z. Liu, G. Zhao, M. Brewer, Q. Lv and E. J. R. Sudhölter, Comprehensive review on surfactant adsorption on mineral surfaces in chemical enhanced oil recovery, *Advances in Colloid and Interface Science*, 2021, **294**, 102467.

9. U. Schwertmann and H. Fechter, *Clay Minerals*, 1982, **17**, 471-476.

10. G. A. Parks, The Isoelectric Points of Solid Oxides, Solid Hydroxides, and Aqueous Hydroxo Complex Systems, *Chemical Reviews*, 1965, **65**, 177-198.

11. CEM, CEM MARS 6 Method Note: Microwave Digestion of Ferric Oxide in iPrep, (accessed August 9, 2023).

12. Nanoparticle Ultrafiltration (Millipore Sigma Technical Paper), https://www.sigmaaldrich.com/US/en/technical-documents/technical-article/analytical-chemistry/filtration/nanoparticle-ultrafiltration, (accessed October 2023).

13. Technical Overview and Performance Capability of the Agilent 7900s ICP-MS for Semiconductor Applications (Agilent White Paper), https://www.agilent.com/cs/library/whitepaper/public/whitepaper_semicon_icp-ms_7900s_5994-1840en_us_agilent.pdf, (accessed October 2023).

14. T. Echigo, D. M. Aruguete, M. Murayama and M. F. Hochella Jr., Influence of size, morphology, surface structure, and aggregation state on reductive dissolution of hematite nanoparticles with ascorbic acid, *Geochimica et Cosmochimica Acta*, 2012, **90**, 149-162.

15. I. V. Chernyshova, A. E. Madden and M. F. Hochella Jr., Size-Dependent Structural Transformations of Hematite Nanoparticles. 1. Phase Transition, *Physical Chemistry Chemical Physics*, 2007, **9**, 1736-1750.

16. R. T. Downs and M. Hall-Wallace, The American Mineralogist Crystal Structure Database, *American Mineralogist*, 2003, **88**, 247-250.

17. E. N. Maslen, V. A. Streltsov, N. R. Streltsova and N. Ishizawa, Synchrotron X-ray Study of the Electron Density in alpha-Fe203, *Acta Crystallographica Section B*, 1994, **B50**, 435-441.

18. I. Persson, Ferric Chloride Complexes in Aqueous Solution: An EXAFS Study, *Journal of Solution Chemistry*, 2018, **47**, 797-805.

19. D. G. Strawn, H. L. Bohn and G. A. O'Connor, *Soil Chemistry 5th Edition*, John Wiley and Sons Ltd., Oxford, UK, 2020.

20. M. Kosmulski, Isoelectric points and points of zero charge of metal (hydr)oxides: 50 years after Parks' review, *Advances in Colloid and Interface Science*, 2016, **238**, 1-61.

21. D. F. Williams and J. C. Berg, The Aggregation of Colloidal Particles at the Air-Water Interface, *Journal of Colloid and Interface Science*, 1992, **152**, 218-228.

22. M. Amadu and A. Miadonye, Determination of the Point of Zero Charge pH of Borosilicate Glass Surface Using Capillary Imbibition Method, *International Journal of Chemistry*, 2017, **9**, 67-84.

23. S. K. Parida, S. Dash, S. Patel and B. K. Mishra, Adsorption of organic molecules on silica surface, *Advances in Colloid and Interface Science*, 2006, **121**, 77-110.

24. R. Atkin, S. J. Craig and S. Biggs, Adsorption Kinetics and Structural Arrangements of Cationic Surfactants on Silica Surfaces, *Langmuir*, 2000, **16**, 9374-9380.

25. W. A. Ducker and E. J. Wanless, Adsorption of Hexadecyltrimethylammonium Bromide to Mica: Nanometer-Scale Study of Binding Site Competition, *Langmuir*, 1999, **15**, 160-168.

26. F. Bresme and M. Oettel, Nanoparticles at fluid interfaces, *Journal of Physics: Condensed Matter*, 2007, **19**, 413101.

27. H. Vatanparast, F. Shahabi, A. Bahramian, A. Javadi and R. Miller, The Role of Electrostatic Repulsion on Increasing Surface Activity of Anionic Surfactants in the Presence of Hydrophilic Silica Nanoparticles, *Scientific Reports*, 2018, **8**, 7251.

28. M. Eftekhari, K. Schwarzenberger, A. Javadi and K. Eckert, The influence of negatively charged silica nanoparticles on the surface properties of anionic surfactants: electrostatic repulsion or the effect of ionic strength?, *Physical Chemistry Chemical Physics*, 2020, **22**, 2238-2248.

29. M. Manciu and E. Ruckenstein, Ions near the air/water interface: I. Compatibility of zeta potential and surface tension experiments, *Colloids and Surfaces A: Physicochemical and Engineering Aspects*, 2012, **400**, 27-35.

30. R.-H. Yoon and J. L. Yordan, Zeta-Potential Measurements on Microbubbles Generated Using Various Surfactants, *Journal of Colloid and Interface Science*, 1986, **113**, 430-438.

31. T. Kolarov, R. Yankov, N. E. Esipova, D. Exerowa and Z. M. Zorin, Charge reversal at the air/water interface as inferred from the thickness of foam films, *Colloid and Polymer Science*, 1993, **271**.

32. C. Tian, J. Feng and R. K. Prud'homme, Adsorption dynamics of polymeric nanoparticles at an air-water interface with addition of surfactants, *Journal of Colloid and Interface Science*, 1010, **575**, 416-424.

33. R. M. Barrer and D. M. MacLeod, Activation of montmorillonite by ion exchange and sorption complexes of tetra-alkyl ammonium montmorillonites, *Transactions of the Faraday Society*, 1955, **51**, 1290-1300.

34. L. Zhang, X. Sun, Y. Song, X. Jiang, S. Dong and E. Wang, Didodecyldimethylammonium Bromide Lipid Bilayer-Protected Gold Nanoparticles: Synthesis, Characterization, and Self-Assembly, *Langmuir*, 2006, **22**, 2838-2843.

35. C. H. Tan, Z. J. Huang and G. H. Xu, Rapid determination of surfactant critical micelle concentration in aqueous solutions using fiber-optic refractive index sensing, *Analytical Biochemistry*, 2010, **401**, 144-147.

36. A. P. Ramos, in *Nanocharacterization Techniques: Micro and Nano Technologies*, eds. A. L. Da Roz, M. Ferreira, F. d. L. Leite and O. N. Oliveira Jr., Elsevier Inc., Cambridge, MA USA, 2017, ch. 4, pp. 99-110.

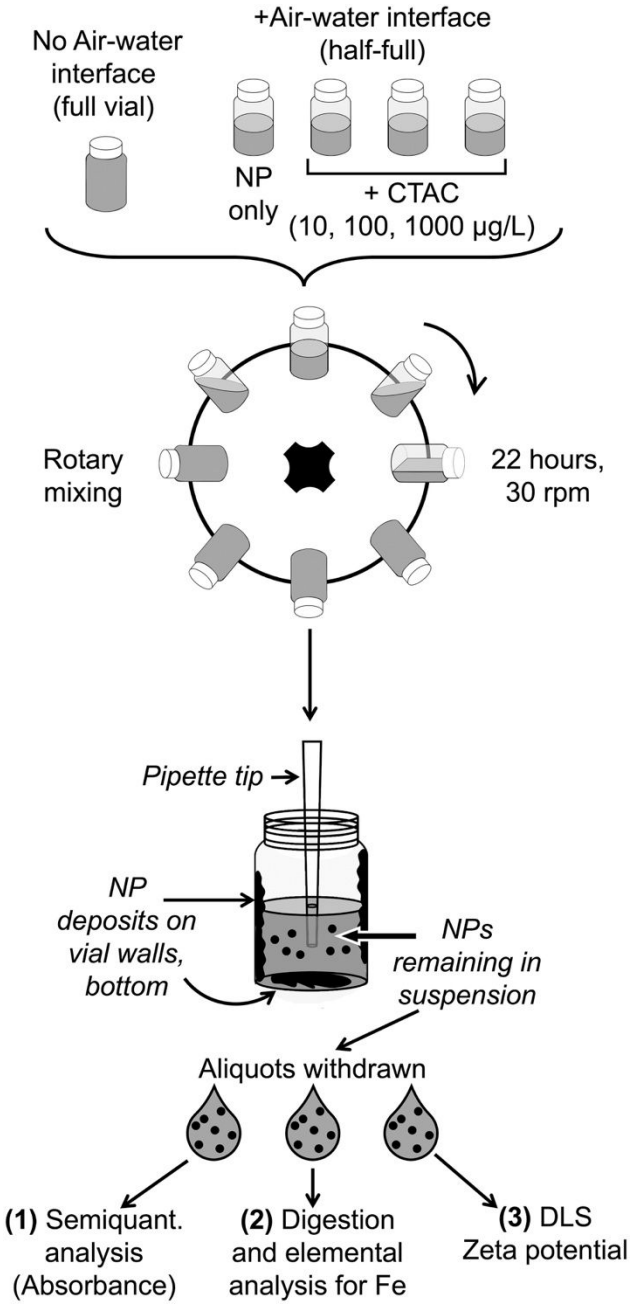

Figure 1. Schematic of experiments. To test the effect of an air-water interface upon the stability of suspended NPs, full (no AWI) and half-full vials (with AWI) of colloidal NP suspensions were prepared (no CTAC added). To test the effect of CTAC on the stability of NP colloids, a series of full and half-full vials were prepared with three concentrations of CTAC: 10, 100 and 1000 µg/L. The vials were subjected to rotary mixing for 22 hours at 30 rpm. Subsequently, to characterize the remaining suspension, aliquots were collected using a pipettor.

The pipette tip was positioned below the air-water interface in the middle of the suspension to avoid NPs on the vial interior or AWI surface. Aliquots were collected for semiquantitative measurement (optical absorption) then elemental analysis or DLS / zeta potential determination.

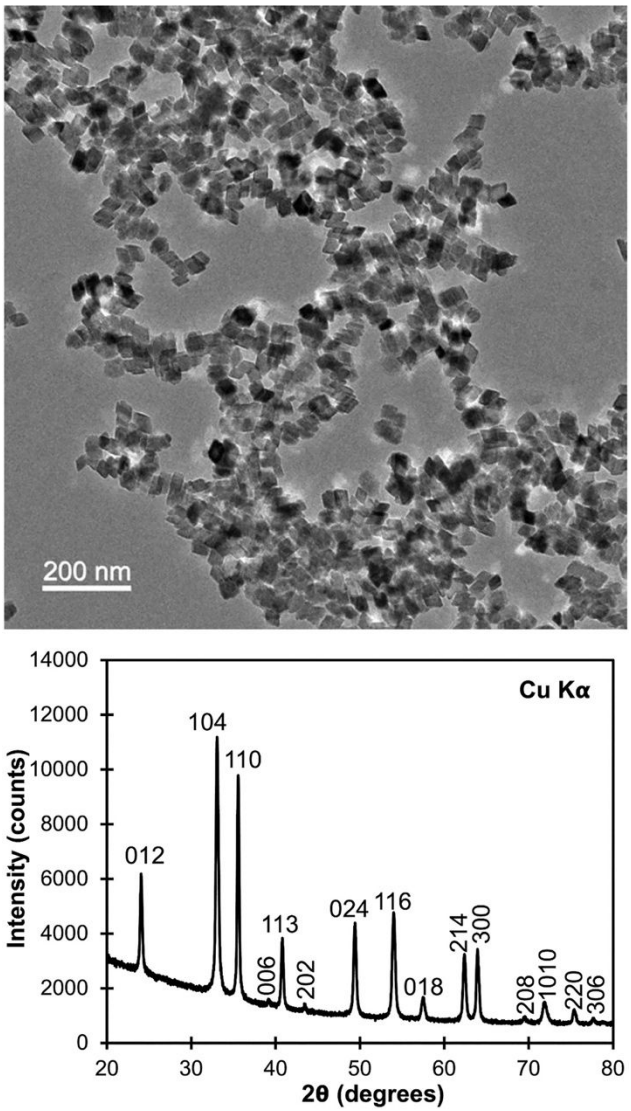

Figure 2. Top: TEM image of hematite nanoparticles; note the rhombohedral morphology. Bottom: Powder XRD from hematite nanoparticles, indexed.

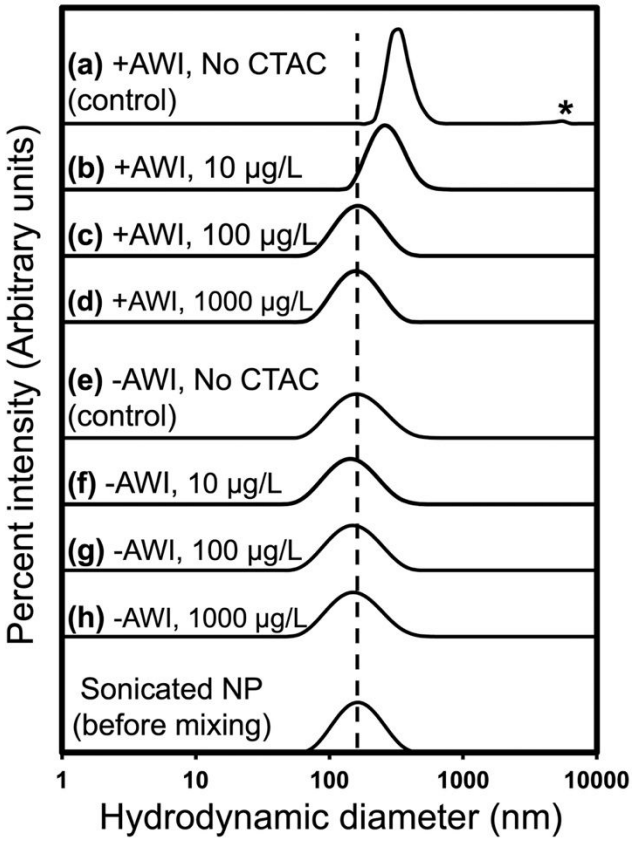

Figure 3. Intensity-based PSDs of NP suspensions from DLS of the following treatments: (a) +AWI without CTAC, (b) – (d) +AWI with [CTAC] = 10, 100, 1000 µg/L, (e) -AWI suspension without CTAC, and (f) – (h) -AWI with [CTAC] = 10, 100, 1000 µg/L. The bottommost PSD is from a freshly-sonicated NP suspension prior to mixing; the dotted line crosses through the maximum value of this curve and is intended to serve as a guide to the eye.

For the +AWI control PSD, an asterisk marks a peak at 4800 nm.

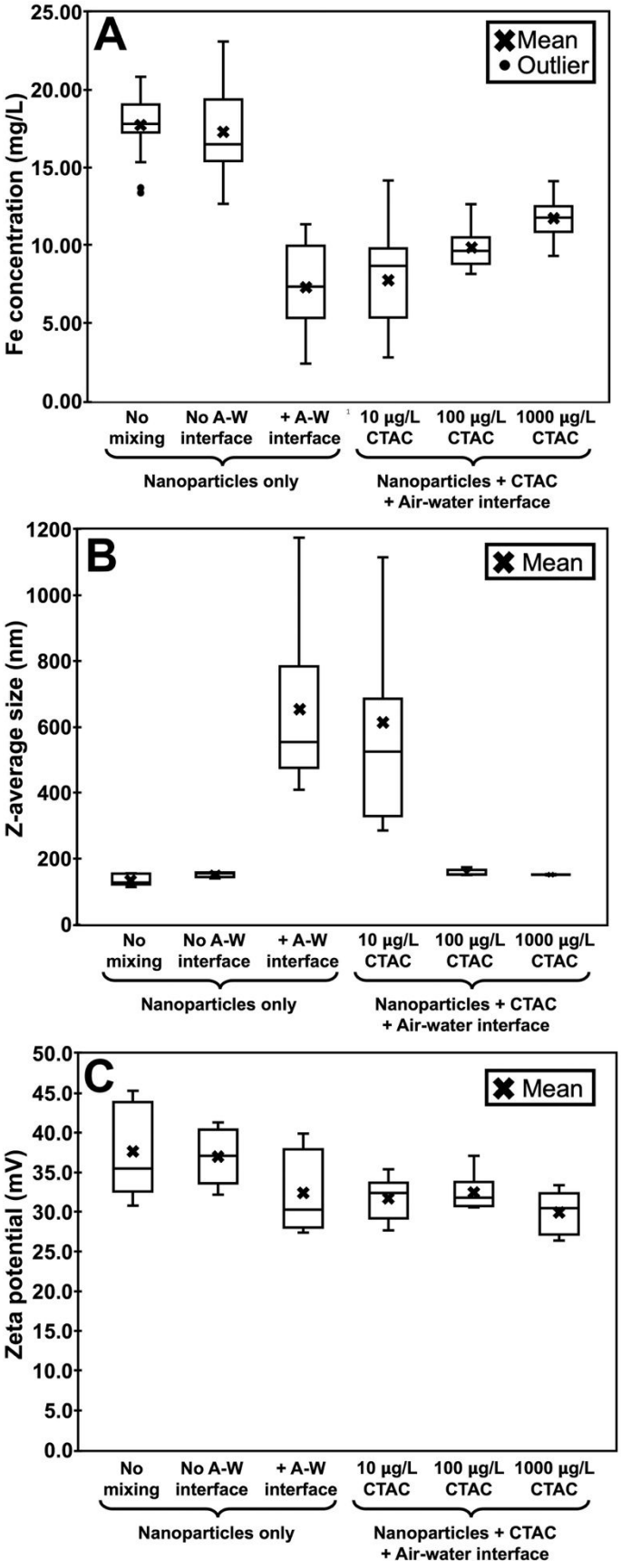

Figure 4. Box-and-whisker plots of characterization data for NP suspensions subjected to different treatments. For all plots, the left three treatments do not contain any CTAC, and the leftmost treatment corresponds to the suspension before mixing. All CTAC-spiked treatments presented are from samples with air-water (A-W) interfaces. (A) [Fe] in suspensions, a proxy for NP stability. Outliers, denoted as round points, are defined as any data lower than Q1 (first quartile value) – 1.5 × (interquartile range). (B) Z-average size (hydrodynamic diameter), and (C) zeta potential. The mean values for each dataset are denoted with X symbols.

Table 1. Chemical characteristics of nanoparticle solutions

[CTAC] (μg/L)	Other sample characteristics	[Fe] (mg / L)	Z-average (hydrodynamic diameter, nm)	PdI	Zeta potential (mV)
0	**Before mixing**	17.65 (± 3.26, *n* = 16)	139.14 (± 18.64, *n* = 15)	0.116 ± 0.016	37.7 (± 6.0 , *n* = 5)
0	**With an air-water interface (+ AWI)**	6.33 (± 2.90, *n* = 42)	655.13 (± 229.16, *n* = 15)	0.550 ± 0.168	32.4 (± 5.2, *n* = 5)
10	**+ AWI**	7.83 (± 2.75, *n* = 22)	282.65 (± 8.06, *n* = 6)	0.198 ± 0.027	31.8 (± 2.6, *n* = 7)
100	**+ AWI**	9.50 (± 1.20, *n* = 26)	156.27 (± 8.92, *n* = 12)	0.105 ± 0.017	32.5 (± 2.4, *n* = 6)
1000	**+ AWI**	11.69 (± 1.25, *n* = 22)	150.39 (± 2.23, *n* = 14)	0.106 ± 0.012	30.0 (± 2.7, *n* = 8)
0	**No air-water interface (-AWI)**	17.30 (± 2.77, *n* = 20)	153.43 (± 7.18, *n* = 6)	0.145 ± 0.021	34.3 (± 2.2, *n* = 6)
10	**-AWI**	21.65 (± 6.48, *n* = 10)	141.38 (± 22.40, *n* = 3)	0.139 ± 0.011	28.3 (± 4.4, *n* = 3)
100	**-AWI**	20.75 (± 5.54, *n* = 10)	139.93 (± 0.61, *n* = 3)	0.129 ± 0.009	25.7 (± 2.6, *n* = 3)
1000	**-AWI**	18.64 (± 5.00, *n* = 12)	130.18 (± 0.61, *n* = 3)	0.130 ± 0.005	32.1 (± 4.4, *n* = 3)

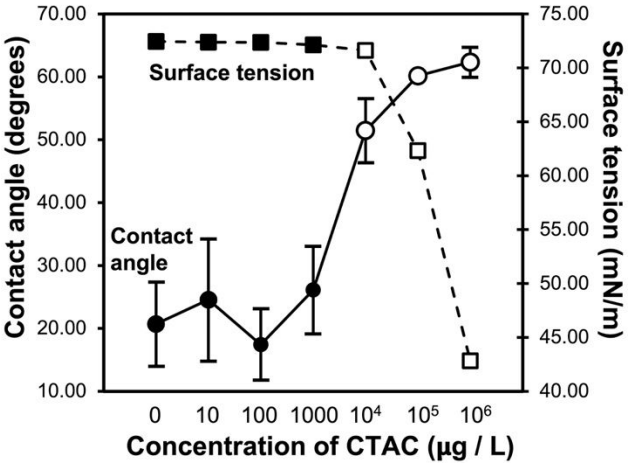

Figure 5. Circles denote the average contact angle values for borosilicate glass exposed to solutions at varying [CTAC]. Error bars indicate standard deviations. Squares denote mean surface tension values at varying [CTAC]. Black-colored points indicate measurements at the [CTAC] used with the NPs (0, 10, 100, 1000 µg/L) and white-colored points indicate measurements at higher [CTAC] not used for NP stability experiments. Mean values and standard deviations are provided in Table 2.

Table 2. Surface tension of CTAC solutions and water contact angles on borosilicate substrates exposed to CTAC solutions

[CTAC] (μg/L)	Mean surface tension (mN/m) ± SD	Mean borosilicate substrate contact angle (degrees) ± SD
0	72.45 (± 0.19)	20.70 (± 6.64)
10	72.39 (± 0.29)	24.56 (± 9.71)
100	72.37 (± 0.40)	17.43 (± 5.65)
1000	72.14 (± 0.19)	26.12 (± 6.95)
10^4	71.61 (± 0.22)	51.46 (± 5.07)
10^5	62.32 (± 0.22)	60.16 (± 0.62)
10^6	42.82 (± 0.07)	62.33 (± 2.37)